ELSEVIER

Nuclear Instruments and Methods in Physics Research B 154 (1999) 174–184

NIM B
Beam Interactions with Materials & Atoms

www.elsevier.nl/locate/nimb

Production of ultra slow antiprotons, its application to atomic collisions and atomic spectroscopy – ASACUSA project

Yasunori Yamazaki [a,b,1]

[a] *Institute of Physics, University of Tokyo, Meguro-ku, Tokyo 153-8902, Japan*
[b] *RIKEN, 2-1 Hirosawa, Wako, Saitama 351-0198, Japan*

Abstract

The Atomic Spectroscopy And Collisions Using Slow Antiprotons (ASACUSA) project aims at studying collision dynamics with slow antiprotons and high precision spectroscopy of antiprotonic atoms. To realize these purposes, the production of high quality ultra slow antiproton beams is essential, which is achieved by the combination of antiproton decelerator (AD) from 3 GeV to 5 MeV, a radio frequency quadrupole (RFQ) decelerator from 5 MeV to 50 keV, and finally an electromagnetic trap from 50 keV to 10 eV. From the atomic physics point of view, an antiproton is an extremely heavy electron and/or a negatively charged proton, i.e., the antiproton is a unique tool to shed light on collision dynamics from the other side of the world. In addition to this fundamentally important feature, the antiproton has also a big practical advantage, i.e., it annihilates with the target nuclei emitting several energetic pions, which provides high detection efficiency with very good time resolution. Many-body effects which are of great importance to several branches of science will be studied through ionization and antiprotonic atom formation processes under single collision conditions. Various antiprotonic atoms including protonium ($\bar{p}p$) are expected to be meta-stable in vacuum, which is never true for those in dense media except for antiprotonic helium. High precision spectroscopy of protonium will for the first time become feasible benefited by this meta-stability. The present review reports briefly the production scheme of ultra slow antiproton beams and several topics proposed in the ASACUSA project.

PACS: 36.10.-k; 34.90.+q; 21.45.+v; 06.20.Jr
Keywords: Ultra slow antiproton and its collision; Few body system; Antiprotonic atom; Fundamental constants

1. Introduction

The Atomic Spectroscopy And Collisions Using Slow Antiprotons (ASACUSA) project [1] has been organized to study various aspects of atomic physics utilizing slow and ultra-slow antiprotons, which is realized by developing ultra slow antiproton beams (10 eV–10 keV) by the combination of the CERN Antiproton Decelerator (AD), an radio frequency quadrupole (RFQ) post-decelerator and an antiproton trap. The schedule in the first several years is summarized in

[1] Tel.: +81-3-5454-6521; fax: +81-3-5454-6433; e-mail: yasunori@phys.c.u-tokyo.ac.jp

0168-583X/99/$ – see front matter
PII: S0168-583X(99)00191-3

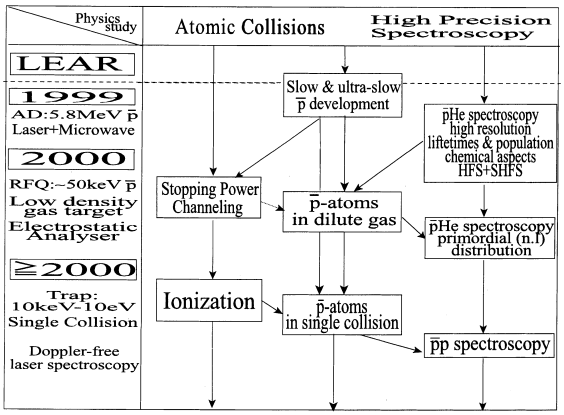

Fig. 1. An overview of the ASACUSA project.

Fig. 1. Such ultra slow antiproton beams allow for the first time: (1) to study ionization and excitation processes in an adiabatic energy range, (2) to study formation processes of various meta-stable antiprotonic atoms ($\bar{p}A^+$) in vacuum, which is never possible in high dense media except for $\bar{p}He^+$ completely surrounded by He, and (3) to make high precision spectroscopy of $\bar{p}A^+$ such as $\bar{p}p$.

When an energetic antiproton interacts with matter, it loses its kinetic energy via collisional ionization and excitation down to the $\sim$ eV region. Then the antiproton is captured into a high-lying atomic orbital of a target atom ($\bar{p}A^+$ formation), and finally annihilates with the target nucleus either via Stark mixing induced by neighboring atoms, or, via cascading down to lower states through Auger and/or radiative transitions. Ionization and excitation are the primary processes to decelerate antiprotons, and are important to comprehensively understand antiproton-matter interactions, which had been studied by PS194 collaboration [2]. However, it was practically impossible to get antiprotons with energies below a few tens keV.

Antiprotonic atoms, i.e., matter–antimatter complexes, have been intensively studied for many years injecting energetic antiprotons into thick targets [3], which was the only way to slow antiprotons down to epithermal energies so that they were ready to be captured into atomic orbitals of the targets. In thick targets, however, the information on the initial stage of $\bar{p}A^+$ formation is smeared out by multiple collisions. Furthermore, the surviving time of $\bar{p}A^+$ has been known to be very short, too short to be measurable, due to perturbation induced by neighboring atoms (molecules), except for $\bar{p}He^+$ in He [4,43,44]. The discovery of meta-stable $\bar{p}He^+$ had opened a new field of $\bar{p}He^+$ spectroscopy, which was developed by the PS205 collaboration. It is then natural to extend the high precision spectroscopy to other $\bar{p}A^+$ atoms. However, no other $\bar{p}A^+$ system is known to be meta-stable in dense media. In order to overcome these difficulties, the combination of slow $\bar{p}$ beams and low density targets is employed in the ASACUSA project, which enables to produce slow isolated $\bar{p}A^+$ in vacuum. The development of ultra slow antiproton beam is therefore essential to study ionizing processes in low energy collisions, the initial stage of the antiprotonic atom formation, and to make high precision spectroscopy of $\bar{p}A^+$. The development of an ultra slow $\bar{p}$ beam is on the line of the former collaboration between PS200 and the group of University of Tokyo, Komaba [5].

It is noted that antiprotons provide a unique possibility to study the behavior of "heavy electron" or "negatively charged proton" at ultra low energies, because other negatively charged heavy particles such as π^- and μ^- have finite lifetimes which are much shorter than the involved cooling times.

2. Production of ultra slow antiproton beam

To materialize the purposes described in the Introduction, the production of a high quality antiproton beam of $\sim$ 10 eV is essential, which is going to be realized via the following five steps as schematically shown in Fig. 2, i.e.

1. Production of $\bar{p}p$ pairs through collisions of 26 GeV/c protons with a production target.
2. Accumulation of 3.5 GeV/c antiprotons, cooling, deceleration down to 0.1 GeV/c (5.3 MeV/u) in the AD (antiproton decelerator), and extraction.
3. Deceleration of the 5.3 MeV antiprotons down to 0–100 keV with the RFQ.

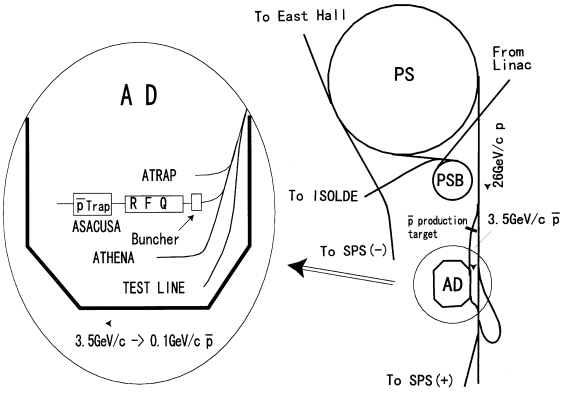

Fig. 2. A schematic drawing of the AD-related proton synchrotron complex at CERN.

4. Injection, trapping, cooling, and (stacking) of several tens keV antiprotons in an electromagnetic trap.
5. Extraction of the cooled antiprotons at around $\sim$ keV as a continuous or a pulsed beam from the trap and transportation to the target area, where the antiprotons are decelerated down to a 10 eV range.

In the first step, antiprotons are produced with 26 GeV/c protons of 1.5×10^{13}/pulse supplied from the CERN PS (proton synchrotron) colliding with a $\bar{p}$ production target (an Ir block of 50 mm thick), which gives an effective antiproton yield of $\sim 3.5 \times 10^{-6}$ $\bar{p}$/p. The momentum distribution of $\bar{p}$ has a broad peak centering at

$$P_{\bar{p}}(\mathrm{GeV}/c) \sim 0.3 P_{p}^{0.8}(\mathrm{GeV}/c), \quad (1)$$

where $P_{\bar{p}}$ and P_{p} are the momenta of the produced antiprotons at the maximum yield and of the incident protons, respectively [6]. In the present case, $P_{\bar{p}}$ is ~ 4 GeV/c, i.e., the $\bar{p}$ energy should be reduced by 9 digits to reach our final goal of the eV $\bar{p}$ beam.

In the second step, the 3.5 GeV/c antiprotons from the production target are accumulated by the AD, cooled and decelerated down to 0.1 GeV/c (5.3 MeV/u), gaining the first 3 digits [7,45]. For stochastic and electron coolings, it takes macroscopic time of ~ 1 min.

In the third step, the 5.3 MeV antiprotons are extracted from the AD as a pulse of $\sim 1 \times 10^{7}$ antiprotons once a minute with the pulse width of ~ 250 ns, transported to the ASACUSA beamline, and then bunched and injected in the RFQ (radio frequency quadrupole) (Fig. 2). The RFQ can accept $\sim 50\%$ of the bunched beam and decelerate it down to 50 keV, gaining another 2 digits. As the electrodes of the RFQ can be floated at ± 50 kV, the energy of antiprotons from the RFQ is in principle tunable from 0 to 100 keV.

In the fourth step, pulsed antiprotons of several tens keV from the RFQ are transported to the electromagnetic $\bar{p}$ trap, guided by a normal conducting solenoid and a superconducting solenoid (5 T) where the $\bar{p}$ trap is installed (see Fig. 3). Transport features of the antiprotons from the RFQ to the trap have been simulated intensively by the RFQ group at CERN. An example of the optimized result is shown in Fig. 3, which tells that the envelope (at 5 standard deviations) of the $\bar{p}$ beam trajectories is compressed down to ~ 2 mm in radius at the center of the solenoid [8]. In order to capture antiprotons with rather low trapping potential, a thin foil is inserted at $z = 87$ cm to reduce the $\bar{p}$ energy below 10 keV as indicated in

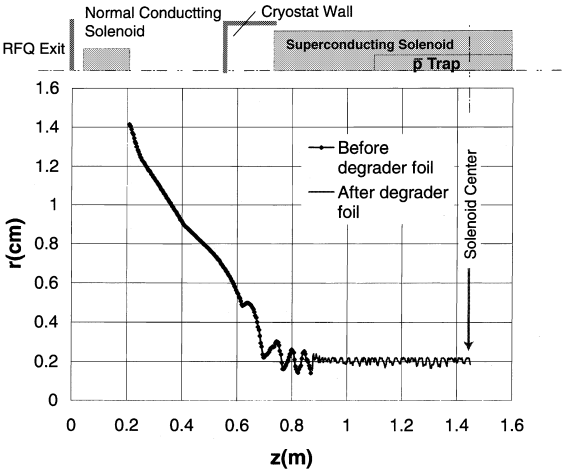

Fig. 3. An envelope (5 standard deviations) of simulated $\bar{p}$ beam trajectories from the RFQ exit to the center of the superconducting solenoid for 63.3 keV antiprotons with the emittance of 10π (courtesy of the RFQ group, CERN) [8]. About 20% of antiprotons from the AD are in the central radial region of ± 1 mm. A degrader foil is set at $z = 87$ cm, which slows 63.3 keV $\bar{p}$ down to around 10 keV. A schematic drawing of the experimental set-up is given at the top of the figure.

the figure. The fraction of "good" antiprotons confined in a region of ~ 1 mm in radius and with energies from 0 to 10 keV amounts to $\sim 40\%$ of antiprotons trapped in the solenoid, i.e., $\sim 20\%$ of those from the AD. As discussed later, the "good" antiprotons refer to those which can be extracted as a high quality beam.

The $\bar{p}$ trap consists of several cylindrical electrodes of 40 mm in inner diameter and total length of ~ 500 mm. At both ends, entrance and exit electrodes are installed to catch energetic antiprotons. At around the center, seven cylindrical electrodes at the center are to form a harmonic potential to stably store and to cool the antiprotons [9]. The end electrode of the trap is biased high enough so that it reflects the pulsed antiprotons back to the entrance of the trap. Before the reflected antiprotons reach the entrance, the bias of the entrance electrode is raised from 0 to >10 kV, which results in trapping the antiprotons. The overall trapping efficiency of the present setup is expected to be about two orders of magnitudes higher than that obtained by the combination of a degrader foil and an electromagnetic trap.

In the harmonic trap, electrons are preloaded, which follow cyclotron motion with an angular frequency, $\omega_{ce}(= eB/m_e \sim 2 \times 10^{11} B\ (\mathrm{T})\ (\mathrm{s}^{-1}))$, and lose their kinetic energy, K_e, via synchrotron radiation with a damping constant γ_{rad} (i.e., $\mathrm{d}K_e/\mathrm{d}t = -\gamma_{rad} K_e$), which is given by

$$\gamma_{rad} = \frac{\mu_0 e^2 \omega_{ce}^2}{3\pi m_e c} \sim 0.4 B\ (\mathrm{T})^2\ (\mathrm{s}^{-1}), \tag{2}$$

where μ_0 is the vacuum permeability. The radiation cooling is practically important only for electrons and positrons because γ_{rad} is inversely proportional to the cube of the particle mass. The wavelength of the corresponding radiation is $\sim 10 B\ (\mathrm{T})^{-1}$ (mm), which is much shorter than the trap size, i.e., the radiation trapping is not very important in the present setup [10]. The electron temperature could be as low as the environmental temperature, which is in the present case 2.3 K. (The solenoid is designed so that the bore temperature is variable from 2.3 to 450 K while keeping the superconducting solenoid at liquid helium temperature.) The cooled electrons then cool the injected antiprotons via the Coulomb interaction in the time range of 10 s [5]. By this way, the remaining 4 digits are gained.

The harmonic trap is designed to confine $\sim 5 \times 10^6$ antiprotons and about 100 times more electrons in a prolate spheroid with a radius ~ 1 mm and its axial length ~ 50 mm, i.e., $\rho_e \sim 5 \times 10^9\ \mathrm{cm}^{-3}$ and $\rho_{\bar{p}} \sim 5 \times 10^7\ \mathrm{cm}^{-3}$.

For such a charged cloud with a temperature below a few eV, the Debye length, $\sqrt{\epsilon_0 k_B T / \sum_i \rho_i e^2}$ (here ϵ_0 is the vacuum dielectric constant, k_B is the Boltzmann constant), is shorter than the size of the cloud, i.e., it behaves as a plasma. The radial electric field of the plasma together with the magnetic field produces an $\mathbf{E} \times \mathbf{B}$ drift rotation [11]. The rotation is governed by the balance of three forces, the electric field due to the space charge, the $\mathbf{E} \times \mathbf{B}$ force, and the centrifugal force. When the plasma is axially symmetric, the angular frequencies of the rotation for electrons and antiprotons, ω_e and $\omega_{\bar{p}}$, are given by

$$\omega_e^{\pm} = \frac{1}{2}\left(\omega_{ce} \pm \sqrt{\omega_{ce}^2 - 2\omega_{pe}^2}\right), \tag{3}$$

$$\omega_{\bar{p}}^{\pm} = \frac{1}{2}\frac{m_e}{m_{\bar{p}}}\left(\omega_{ce} \pm \sqrt{\omega_{ce}^2 - 2\frac{m_{\bar{p}}}{m_e}\omega_{pe}^2}\right), \tag{4}$$

respectively, where ω_{pe} is a plasma angular frequency of the electron, which is defined as

$$\sqrt{(\rho_e + \rho_{\bar{p}})e^2/m_e\epsilon_0} \sim 5 \times 10^4 \sqrt{\rho_e\ (\mathrm{cm}^{-3})}\ (\mathrm{s}^{-1}).$$

The above equations tell that there exists a maximum density that can be confined at a given magnetic field B, which is called the *Brillouin limit*. Furthermore, in the present condition (i.e., $\rho_e \gg \rho_{\bar{p}}$), ρ_e governs the Brillouin limit for antiprotons as well as that for electrons, which are $3 \times 10^9 B\ (\mathrm{T})^2/\mathrm{cm}^3$ and $5 \times 10^{12} B\ (\mathrm{T})^2/\mathrm{cm}^3$, respectively. The solenoid is designed to yield 5 T, which keeps the expected density well-below the Brillouin limit even for antiprotons. In this case, ω_e^+ and $\omega_{\bar{p}}^+$ are approximately given by ω_{ce} and $(m_e/m_{\bar{p}})\omega_{ce}(\equiv \omega_{c\bar{p}})$, respectively, and ω_e^- and $\omega_{\bar{p}}^-$ are

$$\omega_e^- \sim \frac{\omega_{pe}^2}{2\omega_{ce}}\left(1 + \frac{\omega_{pe}^2}{2\omega_{ce}^2}\right), \tag{5}$$

$$\omega_{\bar{p}}^{-} \sim \frac{\omega_{pe}^2}{2\omega_{ce}}\left(1+\frac{m_{\bar{p}}}{m_e}\frac{\omega_{pe}^2}{2\omega_{ce}^2}\right), \tag{6}$$

respectively. For $\rho_e \sim 5\times 10^9/\mathrm{cm}^3$ and $B=5$ T, $\omega_{e(\bar{p})}^{-}$ is $\sim 10^7$/s, i.e., the cooled antiprotons inevitably possess a finite kinetic energy because of this rotation even when they are cooled down to 0 K, which amounts to ~ 0.5 eV for antiprotons at the periphery of the plasma in the present conditions [12]. Eqs. (5) and (6) tell that (1) $\omega_{e(\bar{p})}^{-}$ is proportional to ρ_e/B, i.e., the kinetic energies of antiprotons and electrons due to the rotation are higher for lower B, and (2) $\omega_{\bar{p}}^{-}$ is $\sim 2\%$ larger than ω_e^{-}, which could cause the $\bar{p}$ cloud to be pushed outside of the electron cloud [13]. However, the separation process is expected to evolve only slowly, because (1) the kinetic energy of the electron relative to the proton due to the rotation is extremely small (<mK) as compared with the possible plasma temperature, and (2) the plasma is more or less strongly magnetized (i.e., $\sqrt{3m_{\bar{p}}k_BT}/eB < e^2/(4\pi\epsilon_0 k_BT)$), which reduces the collision frequency between electrons and antiprotons. One of the electrodes near the center of the harmonic trap is segmented into four to apply a rotating electric field on the plasma, which is effective to radially compress the trapped particles [14]. For non-neutral plasmas, various instability modes such as diocotron instability have been known [15]. The control of two component non-neutral plasma is the key issue to effectively trap, cool, and extract antiprotons as a high quality beam.

The vacuum around the trap should be kept high so that the annihilation rate, γ_{ann}, of antiprotons with residual gas is much lower than the cooling rate. In the energy range in question i.e., above several K), the $\bar{p}A^+$ formation cross section, $\sigma_{\bar{p}A^+}$, which eventually leads to $\bar{p}$ annihilation is expected to be much larger than the direct annihilation cross section [16]. Employing $\sigma_{\bar{p}A^+}$ discussed in Section 4, the rate at room temperature is crudely expressed

$$\gamma_{ann} \sim 5\times 10^7 P\ (\mathrm{Torr})\ (\mathrm{s}^{-1}). \tag{7}$$

Eq. (7) tells that the vacuum around the trap should be better than 10^{-11} Torr at room temperature so that $\gamma_{ann} \ll \gamma_{rad}$ holds.

In the fifth step, the cooled antiprotons are extracted at around $\sim$ keV as a continuous or a pulsed beam from the trap and transported to the target area, where the antiprotons are decelerated down to 10 eV range. Several differential pumping stages separated by small holes ($\sim$ 3 mm diameter) are necessary on the way from the trap to the target chamber, to keep the trap area at UHV and at the same time to use a gas cell of 10^{-3} Torr in the target chamber. Simulations of extracted $\bar{p}$ trajectories have shown that the radial distributions of the antiprotons in the trap should be equal to or smaller than ~ 1 mm for a reasonable transportation [17].

3. Ionization

The study of collision dynamics, particularly that of many-body systems, is the least explored and accordingly of great importance for various branches of science. For example, ionizing processes in $\bar{p}$–H collisions provide one of the simplest and accordingly the ideal case to study fundamental aspects of collision dynamics [2,18].

Single ionization cross sections of D are shown in the upper part of Fig. 4. Several recent theoretical predictions are also plotted in the figure [19–21]. It is seen that all the theoretical predictions agree more or less with one another for $\bar{p}$ energies higher than ~ 50 keV as well as with the experimental results. At lower impact energies, although the scatter among different theoretical predictions gets larger, the major theoretical results predict that the cross section becomes almost energy independent, which is qualitatively in accord with the "Fermi–Teller (FT) mechanism" [22]. The idea of the FT mechanism is as follows: When $\bar{p}$ approaches an atom, the binding energy of an outermost electron of the atom gets smaller, and at a certain distance, d_{cr}, the binding energy vanishes (d_{cr} is called the critical distance), i.e., the atom is ionized even when the collision evolves adiabatically as far as the impact parameter is smaller than d_{cr}. It is noted that such a behavior is quite different from the ordinary ion–atom collisions, where the ionization cross section decreases as the projectile velocity decreases unless a

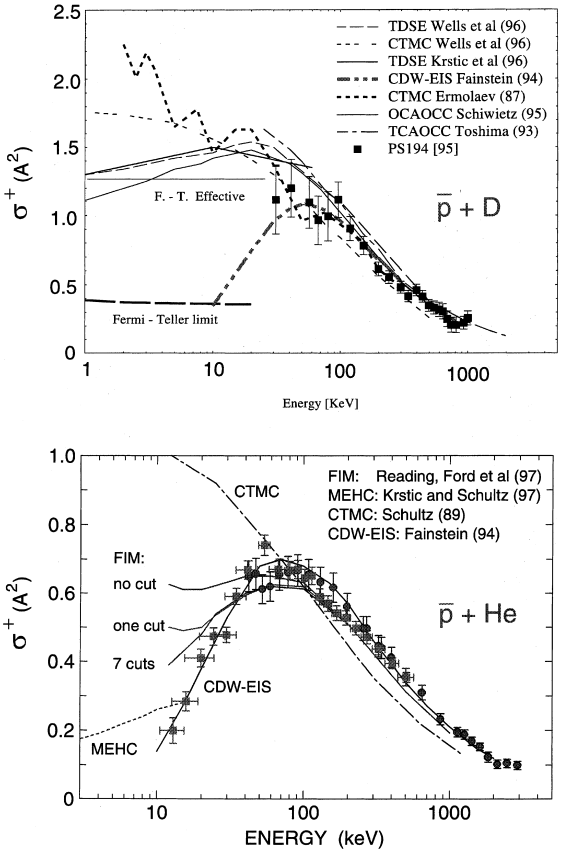

Fig. 4. Single ionization cross sections of D (upper) and He (lower) by antiprotons [2].

resonant charge transfer process comes into play. The adiabatic ionization cross section is expected to have a weak energy dependence and to be $\sim \pi d_{cr}^2$ independent of the $\bar{p}$ energy, which is inferred by the experimental results (the upper part of Fig. 4). However, d_{cr} for H is 0.63 a.u., and the expected ionization cross section is ~ 1.3 a.u., which is about one-third of the experimental findings. Contributions of dynamic effects during adiabatic collisions are under discussion.

The single ionization cross section of He is drawn in the lower part of Fig. 4, which shows a clear peak at ~ 70 keV in contrast to the D target case [23,24]. The behavior of the ionization cross section has been successfully explained by Reading and co-workers [25,46] employing the so-called forced impulse method (FIM). It is noted that the critical distance for He is "negative", i.e., the electronic binding energy stays negative finite even under the unified atom limit, which is known as H^-. Ionization of atoms and molecules with different critical distances will be measured for ultra slow antiprotons to further study the collision dynamics. A kinematically complete ionization experiment of hydrogen and helium by antiprotons is also planned, which is realized by employing the technique of Recoil-Ion Momentum Spectroscopy [26]. Such experiments have become feasible and have recently been performed for slow proton on helium collisions at energies between 5 and 15 keV as well as for heavy-ion impact [27].

The double ionization process of helium by antiproton has been intensively studied, which revealed that $\sigma^{++}(\bar{p})$ is about two times larger than $\sigma^{++}(p)$ of the same velocity even for projectile energies as high as 10 MeV [2]. The FIM method has been successfully applied also for the double ionization process [28] showing that the electron–electron correlation plays an essential role to reproduce the observations. In this direction, the study of double excitation process should be very important, because a collision system with (quasi-)bound states can be handled accurately as compared with those involving two continua like in the case of double ionization, and could be more sensitive to details of the collision dynamics [29,47,48].

The stopping power of $\sim$ keV antiprotons [2], the channeling of ~ 100 keV antiprotons through a single crystal target, etc. will also be studied employing $\bar{p}$ beams from the RFQ and from the trap. As discussed above, the ionization behavior of $\bar{p}$ is quite different from that of p in the energy region under discussion. As a result, the stopping power behavior of $\bar{p}$ is also expected to be quite different from that of p.

4. Capture

When an antiproton with very low kinetic energy ionizes an atom, the $\bar{p}$ can be trapped into an atomic orbital with a large principal quantum number n. The energy conservation before and after the collision in the center of mass system requires,

$$K_{\bar{p}A} - \epsilon_{eA^+} = K_{e(\bar{p}A^+)} - \epsilon_{\bar{p}A^+} \sim K_e - \epsilon_{\bar{p}A^+}, \quad (8)$$

where $K_{AB} \equiv \frac{1}{2}\mu_{AB}v_{AB}^2$, μ_{AB} is the reduced mass of particles A and B, v_{AB} is the relative velocity between A and B, ϵ_{AB} is the binding energy between A and B, and $K_e = \frac{1}{2}m_e v_e^2$ (m_e is the electron mass, and v_e is the velocity of the released electron in the laboratory frame). Because the ionization takes place adiabatically and the electron is oozing out, v_e is expected to be very close to zero [30], i.e.,

$$\epsilon_{\bar{p}A^+}\left(\sim \frac{\mu_{\bar{p}A}}{m_e}\frac{\epsilon_R}{n^2}\right) \sim \epsilon_{eA^+} - K_{\bar{p}A}, \quad (9)$$

where ϵ_R is the Rydberg constant (~ 13.6 eV), and n is the principal quantum number of the $\bar{p}A^+$ ion. For $\bar{p}A^+$ to be formed, $\epsilon_{\bar{p}A^+}$ should be positive. In other words, the trapping cross section is finite when $K_{\bar{p}A}$ satisfies

$$0 < K_{\bar{p}A} < \epsilon_{eA^+}. \quad (10)$$

Eq. (9) tells that the principal quantum number of the formed $\bar{p}A^+$ is a function of $K_{\bar{p}A}$, $n(K_{\bar{p}A})$, which varies from $n_{min}(\sim \sqrt{(\mu_{\bar{p}A}/m_e)(\epsilon_R/\epsilon_{\bar{p}A^+})})$ to ∞ as $K_{\bar{p}A}$ increases from 0 to ϵ_{eA^+}.

The basic mechanism is relatively simple and is expected to be general for atomic collisions involving "heavy electrons" such as μ^-,π^-, K^-, and $\bar{p}$. When a "heavy electron" approaches an atom with its velocity lower than the Bohr velocity, a "molecular" orbital is formed, which leads to an adiabatic electron release. On the way out from the target area, the heavy electron must have enough kinetic energy to overcome the Coulomb potential of the ionized target, i.e., depending on the kinetic energy, the electron release process branches into a simple ionization or into an exotic atom formation.

The dipole polarizability, α, of an atom is of the order of 1 a.u. (e.g., 4.5 a.u. for H and 1.4 a.u. for He), i.e., the interaction of the incident $\bar{p}$ with the induced dipole becomes important for $K_{\bar{p}A}$ of ~ 1 a.u. and lower. The combination of the polarization potential ($=\alpha e^2/2r^4$) and the centrifugal potential causes the $\bar{p}$ to make an orbiting motion, which makes the effective interaction time between the $\bar{p}$ and the atom very long. If some reaction channels are open during the interaction, such reactions are enhanced. A simple argument shows that the cross section of such a reaction is given by $\sigma_L = 2\pi e\sqrt{\alpha/\mu_{\bar{p}A}}/v_{\bar{p}A}$, which is called *Langevin* cross section. In the case of $\bar{p}$ impacts, the electron release process is the corresponding reaction, i.e., the cross section is not constant as was anticipated in the FT model but increases as the energy decreases.

A possible maximum orbital angular momentum of the $\bar{p}A^+$, $l_{max}(K_{\bar{p}A})$, would be $\sim \mu_{\bar{p}A}v_{\bar{p}A}b_{eff} \sim (e\mu_{\bar{p}A})^{1/2}(8\alpha K_{\bar{p}A})^{1/4}$ where b_{eff} is estimated by $b_{eff} = \sqrt{\sigma_L/\pi}$. $l_{max}(K_{\bar{p}A})$ and n are expected to increase monotonically from 0 to $\sim (e\mu_{\bar{p}A})^{1/2}(8\alpha\epsilon_{eA^+})^{1/4}$ and from n_{min} to ∞, respectively, when $K_{\bar{p}A}$ is increased from 0 to ϵ_{eA^+}. It is seen that n needs to be a couple of units bigger than n_{min} in order to populate meta-stable states holding high angular momentum. Quantitative discussions on the behavior of the antiprotonic atom formation processes are given, e.g., in Refs. [31,32].

Quantum theoretical treatments are very difficult because large number of reaction channels are involved. Cohen has employed a Classical Trajectory Monte Carlo (CTMC) method and an Fermion Molecular Dynamics (FMD) method to handle $\bar{p} + H$ and H_2 collisions in a low energy region [33,34,49]. Fig. 5 shows the prediction of the FMD simulation for $\bar{p}$ + H and $\bar{p}$ + H_2. The heavy solid line and the heavy dashed line shows protonium ($\bar{p}p$) formation cross section, $\sigma_{\bar{p}p}$, and total (formation and ionization) cross section, σ_t, in $\bar{p}$–H collisions, respectively. A clear threshold is seen at around 0.5 a.u. for $\sigma_{\bar{p}p}$ although σ_t varies smoothly. The CTMC calculation predicts that the average values of n and l are around 100 and 35, respectively at $K_{\bar{p}H} = 0.5$ a.u. [33,49]. These results are consistent with what are expected from the qualitative discussions given above.

Among various antiprotonic atoms, protonium is particularly interesting because it is the simplest two body system consisting of a particle and an antiparticle involving the strong interaction. Such a two body system in Yrast states can decay only via slow radiative transitions when the external electric field is negligible, and its lifetime can be much longer than 1 μs, i.e., a high resolution laser

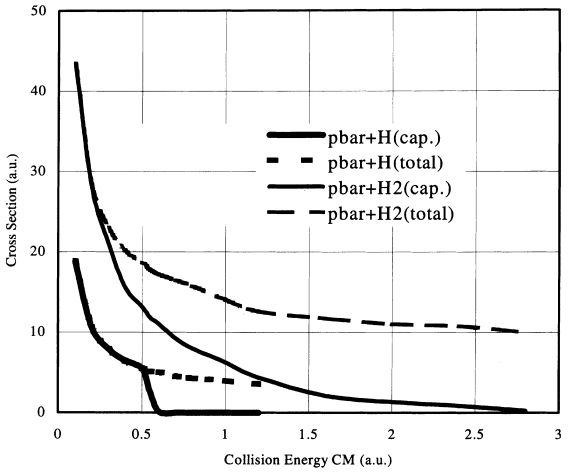

Fig. 5. Total (dashed lines) and capture (solid lines) cross sections of antiprotons in collision with H (heavy lines) and H_2 (light lines) atoms [33,49].

spectroscopy becomes applicable to $\bar{p}p$ for the first time.

In the case of molecular targets, the electron release process leads to a temporary formation of an antiprotonic molecule, which then dissociates into an antiprotonic atom and a residual atom (ion). The initial internal motion of the molecule plays an important role in the antiprotonic atom formation process, and the residual atom (ion) takes care not only of the energy balance but also of the momentum balance. Because of this, the $\bar{p}A^+$ formation cross section stays finite even beyond the threshold energy given in Eq. (10). The light solid line and the light dashed line in Fig. 5 show the formation and total (ionization + formation) cross sections, respectively [33,49]. A dramatic increase of $\sigma_{\bar{p}p}$ for an H_2 target is predicted far beyond the threshold. Further, molecular targets provide an interesting chance to study a "dynamic Stark effect". The temporary antiprotonic molecule described above will dissociate into an antiprotonic atom and a spectator atom (ion), i.e., the antiprotonic atom evolves in the electric field of the spectator atom (ion) for a finite time. The electric field will increase the fraction of *s*-state components due to Stark mixing, and accordingly increase the annihilation rate, which may provide a new and sensitive measure of collision dynamics. Experiments with H_2 and D_2 targets are under preparation to study the isotope effects predicted in Ref. [35].

Various multi-electron antiprotonic atoms are also expected to have intrinsic meta-stability, which can be exclusively realized only when they are produced under single collision conditions isolated in vacuum except for $\bar{p}He^+$. Like in the case of H, Li has a positive critical distance for $\bar{p}$ ($d_{cr} = 0.79$ a.u) [36]. As the $\bar{p}$ replaces the 2s electron of Li, it is far outside of the residual two 1s electrons, i.e., the Auger transition rates will be fairly small because the transition energies are large and the spatial overlap between the initial and the final orbits is small. It is further noted that the antiprotonic states with the same principal quantum number but with different orbital angular quantum numbers do not degenerate, i.e., $\bar{p}Li^+$ is stable against annihilation induced by electric fields.

From Eq. (9), a possible smallest principal quantum number, n_{min}, of the formed $\bar{p}Li^+$ is estimated to be ~ 62–63, considering the binding energy of Li 2s electron being ~ 5.4 eV. The right half of Fig. 6 shows the correlation diagrams of $\bar{p}Li^+$ for $l = 60$–64 and $\bar{p}Li^{++}$ for $l = 37$ and 38 [36]. As is seen, there is practically no spatial overlap between $\bar{p}Li^+$ states and $\bar{p}Li^{++} + e$ states, i.e., the formed $\bar{p}Li^+$ can de-excite only radiatively. A naive consideration indicates that such a meta-stability could be a general aspect of the $\bar{p}A^+$ if it is isolated in vacuum and if for example A is an atom of alkali metal. As a reference, the correlation

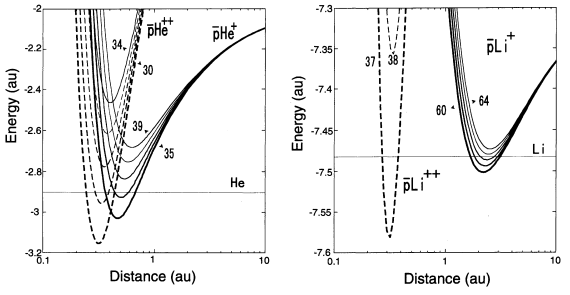

Fig. 6. Correlation diagrams of (1) $\bar{p}$–He^+ ($l = 35$–39) and $\bar{p}$–He^{++} (left), and (2) $\bar{p}$–Li^+ ($l = 60$–64) and $\bar{p}$–Li^{++} ($l = 37$–38) (right). The solid straight lines show energy levels of neutral He (left) and Li (right) [36].

diagrams of $\bar{p}He^{+}$ for $l = 35$–39 and $\bar{p}He^{++}$ for $l = 30$–34 are given in the left half of Fig. 6, which shows a considerable overlap between $\bar{p}$ wavefunctions before and after the Auger decay, indicating that the Auger rates could be very sensitive on n and l as they actually are [4,43,44].

The annihilation of $\bar{p}He^{++}$ was used as the important monitor of the laser spectroscopy of $\bar{p}He^{+}$, because $\bar{p}He^{++}$ has no electron shield and is very weak against external electric fields, i.e., it annihilates immediately after it is produced in dense media, which has been used as an indicator of the transition. This does not work any more if $\bar{p}He^{++}$ is in vacuum, and a single collision between $\bar{p}$ and He could prepare not only meta-stable $\bar{p}He^{+}$ but also meta-stable $\bar{p}He^{++}$ via an autoionizing process. A similar process will be effective to produce a meta-stable antiprotonic ion $\bar{p}A^{++}$) using alkali earth. Such an antiprotonic ion (e.g. $\bar{p}Be^{++}$) has a closed electron shell, and accordingly the spatial overlap of the electrons with the $\bar{p}$ is small, which again decays primarily via radiation and is strong against external electric field. It might be stored even in a trap. Furthermore, if e.g., $\bar{p}C^{+}$ is prepared in a meta-stable state, the interaction between the $\bar{p}$ spin magnetic moment and the 2p electron orbital magnetic moment could be studied, which gives another way to study the $\bar{p}$ magnetic moment.

5. $\bar{p}A^{+}$ spectroscopy

The discovery of meta-stable $\bar{p}He^{+}$ has made it possible to study the nature of antiprotonic atoms with high precision laser spectroscopy [4,37,43,44]. This field has developed rapidly from the level of identification of the principal and angular momentum quantum numbers (i.e., n and l) to the level of determination of the transition energies with a fraction of ppm [38], which agrees within a few ppm accuracy with theoretical predictions, where relativistic and the Lamb shift corrections of the electron are taken into account [39–41]. The above finding tells that if the theoretical treatment of the Coulomb three-body system is correct, the CPT invariance has been proved with the ppm accuracy, particularly regarding the antiproton mass and/or the antiproton charge. In the upper part of Fig. 7 a resonance profile observed for the antiprotonic $(n, l) = (37, 35) \rightarrow (38, 34)$ transition is plotted, which clearly shows a doublet structure [37]. This is because each (n, l) energy level of the antiprotonic atom splits into several ones due to the interaction among the magnetic moments carried by electrons, antiprotons, and also target nucleus. In the case of $\bar{p}He^{+}$, the interaction between the electron spin, $\boldsymbol{s}_e$, and the orbital angular momentum of antiproton, $\boldsymbol{l}_{\bar{p}}$, is the most important,

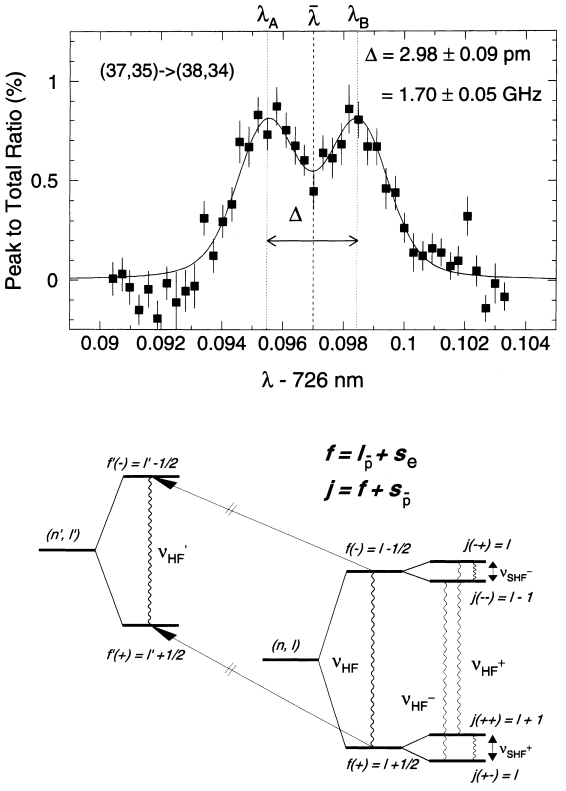

Fig. 7. Upper: High resolution resonance profile of the (37,35) $\rightarrow$ (38,34) transition of $\bar{p}$–He^{+}. Lower: A schematic diagram showing level splittings due to interaction between the orbital magnetic moment of $\bar{p}$ and the spin magnetic moment of electron, $\boldsymbol{l}_{\bar{p}} \cdot \boldsymbol{s}_e$, and that between the $\bar{p}$ spin magnetic moment and the rest, $\boldsymbol{s}_{\bar{p}} \cdot (\boldsymbol{l}_{\bar{p}} + \boldsymbol{s}_e)$. It is predicted that the splitting due to $\boldsymbol{l}_{\bar{p}} \cdot \boldsymbol{s}_e$ is $\nu'_{HF} = 11.1$ GHz and $\nu^{\pm}_{HF} = 12.9$ GHz for (37,35) and (38,34), respectively, and the splitting due to $\boldsymbol{s}_{\bar{p}} \cdot (\boldsymbol{l}_{\bar{p}} + \boldsymbol{s}_e)$, is $\nu^{-}_{SHF} = 130$ MHz, $\nu^{+}_{SHF} = 160$ MHz [42]. The observed splitting seen in the upper figure is consistent with $\nu^{\pm}_{HF} - \nu'_{HF}$.

and then that between $\boldsymbol{f}$ ($\equiv \boldsymbol{s}_e + \boldsymbol{l}_{\bar{p}}$) and the antiproton spin, $\boldsymbol{s}_{\bar{p}}$, the relative importance of which is schematically shown in the lower part of Fig. 7 [42]. The hyperfine splittings will be intensively studied employing laser & microwave resonances, which gives the magnetic moment of $\bar{p}$. $\bar{p}A^+$ spectroscopy of the second generation will start soon with the development of slow $\bar{p}$ beams and $\bar{p}p$ production in vacuum.

Acknowledgements

The author is deeply indebted to K. Ohtsuki, A. Lombardi, H. Totsuji, J. Cohen, G. Korenman, and colleagues of the ASACUSA project, particularly T. Azuma, R.S. Hayano, H. Higaki, H. Knudsen, K. Komaki, A. Mohri, E. Widmann and T. Yamazaki for their fruitful and vivid discussions. The work is supported by the Grant-in-Aid for Creative Basic Research (10NP0101), Ministry of Education, Science, and Culture.

References

[1] ASACUSA collaboration proposal, 1997 CERN/SPSC 97-19, SPSC P-307.
[2] H. Knudsen, J. Reading, Phys. Rep. 212 (1992) 107.
[3] C.J. Batty, Rep. Prog. Phys. 52 (1989) 1165.
[4] T. Yamazaki et al., Nature 361 (1993) 238.
[5] X. Feng, M.H. Holzscheiter, M. Charlton, J. Hangst, N.S.P. King, R.A. Lewis, J. Rochet, Y. Yamazaki, Hyperfine Interactions 109 (1997) 145.
[6] D. Moehl, Hyperfine Interactions 109 (1997) 33.
[7] AD is under construction and will be ready in 1999 to replace LEAR. For a historical review, see J. Eades, F.J. Hartmann, Rev. Mod. Phys., to be published.
[8] A. Lombardi, Private communication.
[9] A. Mohri, H. Higaki, H. Tanaka, Y. Yamazawa, M. Aoyagi, T. Yuyama, T. Michishita, Jpn. J. Appl. Phys. 37 (1998) 664.
[10] R.S. Van Dyck Jr., P.B. Schwinberg, H.G. Dehmelt, Atomic Physics 9 (1984) 53.
[11] T.M. O'Neil, in: C.W. Roberson, C.F. Driscoll (Eds.), Non-Neutral Plasma Physics, American Institute of Physics, New York, 1988, p. 1.
[12] It is seen that the kinetic energy due to the plasma rotation is fairly large, which should be fully taken into account in considering the production and trapping of ultra cold antihydrogen by a nested trap (As antiprotons and positrons are co-rotating in the same direction with roughly the same angular frequency (see Eqs. (5) and (6)), the production rate is primarily governed by the plasma temperature).
[13] D.J. Larson, J.C. Bergquist, J.J. Bollinger, W.M. Itano, D.J. Wineland, Phys. Rev. Lett. 57 (1986) 70.
[14] X.-P. Huang, F. Anderegg, E.M. Hollmann, C.F. Hollmann, T.M. O'Neil, Phys. Rev. Lett. 78 (1997) 875.
[15] R.C. Davidson, Physics of Non-neutral Plasmas, Addison Wesley, 1990.
[16] W.R. Gibbs, Phys. Rev. A 56 (1997) 3553.
[17] T. Ichioka, Master Thesis, University of Tokyo, 1996.
[18] H. Knudsen, U. Millelson, K. Paludan, K. Kirsebom, S.P. Moeller, E. Uggehoej, J. Slevin, M. Charlton, E. Morenzoni, Phys. Rev. Lett. 74 (1995) 4627.
[19] N. Toshima, Phys. Lett. A 175 (1993) 133.
[20] P.S. Krstic, D.R. Schultz, R.K. Janev, J. Phys. B 29 (1996) 1941.
[21] J.C. Wells, D.R. Schultz, P. Gravras, M.S. Pindzola, Phys. Rev. A 54 (1996) 593.
[22] E. Fermi, E. Teller, Phys. Rev. 72 (1947) 399.
[23] P. Hvelplund, H. Knudsen, U. Mikkelsen, E. Morenzoni, S.P. Moeller, J.O.P. Pedersen, S. Tang-Petersen, E. Uggerhoej, T. Worm, J. Phys. B 27 (1994) 925.
[24] L.H. Andersen, P. Hvelplund, H. Knudsen, S.P. Moeller, J.O.P. Pedersen, S. Tang-Petersen, E. Uggerhoej, K. Elsener, E. Morenzoni, Phys. Rev. A 41 (1990) 6536.
[25] J. Reading, T. Bronk, A.L. Ford, L.A. Wehrman, K.A. Hall, J. Phys. B 30 (1997) L189.
[26] J. Ullrich, R. Moshammer, R. Doerner, O. Jagutzuki, V. Mergel, H. Schmidt-Boecking, L. Spielberger, J. Phys. B 30 (1997) 2917.
[27] R. Doerner, H. Kehmliche, M.H. Prior, L.C. Cocke, J.A. Gary, R.E. Olson, V. Mergel, J. Ullrich, H. Schmidt-Boecking, Phys. Rev. Lett. 77 (1996) 4520.
[28] A.L. Ford, J. Reading, J. Phys. B 27 (1994) 4215.
[29] T. Morishita, K. Hino, S. Watanabe, M. Matsuzawa, Phys. Rev. A 53 (1996) 2345.
[30] V.K. Dolinov, G.Ya. Korenman, I.V. Moskalinko, V.P. Popov, Muon Catalyzed Fusion 4 (1989) 169.
[31] G.Ya. Korenman, Hyperfine Interactions 101/102 (1996) 81.
[32] J.S. Cohen, Electromagnetic Cascade and Chemistry of Exotic Atoms, p1, L.M. Simons et al., (Ed.), Plenum Press, New York, 1990.
[33] J.S. Cohen, Phys. Rev. A 56 (1997) 3583.
[34] J.S. Cohen, N.T. Padial, Phys. Rev. A 41 (1990) 3460.
[35] J.S. Cohen, Phys. Rev. A, to be published.
[36] K. Ohtsuki, private communication.
[37] E. Widmann et al., Phys. Lett. B 404 (1997) 15.
[38] H.A. Torii, et al., Phys. Rev. A 59, to be published.
[39] V.I. Korobov, Phys. Rev. Lett., to be published.
[40] N. Elander, E. Yarevsky, Phys. Rev. A 56 (1997) 1855.
[41] Y. Kino, M. Kamimura, H. Kudo, in: Proceedings of the 15th International Conference on Few-Body Problems in Physics, Groningen, 1997.
[42] D. Bakalov, V.I. Korobov, Phys. Rev. A 57 (1998) 1662.
[43] N. Morita et al., Phys. Rev. Lett. 72 (1994) 1180.

[44] R.S. Hayano et al., Phys. Rev. A 55 (1997) 1.
[45] J. Eades, CERN Courier 44 (1998) 5674.
[46] T. Bronk, J.F. Reading, A.L. Ford, J. Phys. B 31 (1998) 2477.
[47] A.L. Godunov, J.H. McGuire, V.A. Schipakov, J. Phys. B 30 (1997) 3227.
[48] V.A. Sidorovich, J. Phys. B 30 (1997) 2187.
[49] J.S. Cohen, private communication.